Nearshore Wave Modeling with High-Order Boussinesq-Type Equations

Patrick J. Lynett[1]

Abstract: The accuracy of using high-order Boussinesq-type models as compared to the typical order models is examined in this paper. The high-order model used is the two-layer model of Lynett and Liu in 2004, which captures both linear and nonlinear wave evolution up to $kh \approx 6$. The physical situations examined all involve nearshore breaking, and an eddy-viscosity type breaking model is adopted for the two-layer model. One-horizontal dimension setups are the focus of this paper. It is shown that high-order models show significant benefit very near to the breaker line. For regular incident waves, the overshoaling seen in the one-layer ("fully nonlinear" extended Boussinesq) model is due to rapid increase of energy in the fifth and higher harmonics. These high-order nonlinear components are captured well in the two-layer model. The two-layer model also exhibits a noticeable accuracy increase for cnoidal waves breaking on a slope. For regular wave evolution over a bar, the high-order models are in good agreement with experiment, correctly modeling the free short waves behind the step. Under irregular wave conditions, it is likewise shown that high-order nonlinearity is important near the breaker line and the outer surf zone. Using SwashX field data, spectral comparisons are made and discussed.

DOI: 10.1061/(ASCE)0733-950X(2006)132:5(348)

CE Database subject headings: Breaking waves; Boussinesq equations; Nearshore; Hydrologic models.

Introduction

Due to present computational constraints, time-domain modeling of large-scale wave evolution in the nearshore zone requires approximate equations. Boussinesq-type equations are becoming increasingly popular for this task. In the past decade, these equations have been used to accurately predict wave evolution across large basins (Basterretxea et al. 2004), wave breaking over irregular topography, wave–structure interaction (Lynett et al. 2000), and wave-induced current patterns (Chen et al. 2003) among many others.

Initial formulations, based on the depth-averaged velocity, were somewhat limited in their description of wind waves in the nearshore. These models generally had good linear accuracy to $kh \approx 1$, but could not yield accurate predictions in the intermediate water regime. Manipulations of the Boussinesq derivation, initiated by Madsen and Sorensen (1992) and Nwogu (1993), led to final model equations with good accuracy through intermediate water. Further nonlinear improvements (e.g., Liu 1994; Wei et al. 1995; Kennedy et al. 2001) made the model even more useful for coastal modeling. However, as noted in Beji and Battjes (1994) and others, even these equations sometimes yielded incorrect predictions, in particular in highly nonlinear situations where, due to bathymetry changes, locked nonlinear components become free. For these scenarios, and in general for a more robust prediction, higher-order accuracy is needed.

[1]Professor, Dept. of Civil Engineering, Texas A&M Univ., College Station, TX 77843-3136. E-mail: plynett@tamu.edu

Note. Discussion open until February 1, 2007. Separate discussions must be submitted for individual papers. To extend the closing date by one month, a written request must be filed with the ASCE Managing Editor. The manuscript for this paper was submitted for review and possible publication on February 18, 2005; approved on August 4, 2005. This paper is part of the ***Journal of Waterway, Port, Coastal, and Ocean Engineering***, Vol. 132, No. 5, September 1, 2006. ©ASCE, ISSN 0733-950X/2006/5-348–357/$25.00.

A handful of high-order Boussinesq-type models exist. Madsen et al. (2002), based on the approach of Agnon et al. (1999), developed a model with excellent linear and nonlinear accuracy in very deep water ($kh \approx 40$). Gobbi et al. (2000) expanded Nwogu's approach to the next order in $(kh)^2$, creating a model with linear accuracy into deep water and nonlinear accuracy throughout intermediate water. Lynett and Liu (2004a) presented the multilayer concept, where the water column is divided into same-fluid "layers" or segments of the water column governed by matched, but unique polynomials describing the horizontal flow field. The two-layer version shows linear and nonlinear accuracy to $kh \approx 6$, while the three and four layer models have good linear accuracy to $kh \approx 17$ and 30, respectively (Lynett and Liu 2004b). Simulations with these high-order models indicate that many nearshore setups benefit from the increased accuracy. High-order model applications involving wave breaking have not been examined to a substantial degree; one such investigation is reported in Sorensen et al. (1999).

In the first section of this paper, the theoretical and numerical aspects of the two-layer model are presented and discussed. Experimental comparisons of wave breaking on a constant slope are given, with the purpose of validating the wave breaking model in both the typical and high-order models. Wave height and setup profiles are examined. Next, one-horizontal-dimension (1HD) wave breaking over a bar is compared. Concluding the comparisons is a recreation of a field experiment.

Two-Layer Model

The high-order simulations presented in this paper employ the two-layer model of Lynett and Liu (2004a). The water column is divided into two same fluid layers, where velocity and pressure are matched at the interface. Within each layer, a unique quadratic polynomial is used to describe the vertical profile of the

horizontal velocity. The multi-layer concept is described as a piecewise matching of polynomials through the water column, where the matching location represents the "interface" between two "layers." The resulting equation model consists of a continuity equation, a momentum equation for the upper layer, and a matching equation for the velocity in the lower layer. These equations are given below

$$\frac{\partial \zeta}{\partial t} + \nabla \cdot [(\zeta - \eta)\mathbf{u}_1 + (\eta + h)\mathbf{u}_2] - \nabla \cdot \left\{ \left[\frac{\eta^3 + h^3}{6} - \frac{(\eta + h)\kappa_2^2}{2} \right] \times \nabla S_2 + \left[\frac{\eta^2 - h^2}{2} - (\eta + h)\kappa_2 \right] \nabla T_2 \right\} - \nabla \cdot \left\{ \left[\frac{\zeta^3 - \eta^3}{6} - \frac{(\zeta - \eta)\kappa_1^2}{2} \right] \nabla S_1 + \left[\frac{\zeta^2 - \eta^2}{2} - (\zeta - \eta)\kappa_1 \right] \nabla T_1 \right\} = 0 \tag{1}$$

$$\frac{\partial \mathbf{u}_1}{\partial t} + \frac{1}{2} \nabla (\mathbf{u}_1 \cdot \mathbf{u}_1) + g \nabla \zeta + \frac{\partial}{\partial t} \left[\frac{\kappa_1^2}{2} \nabla S_1 + \kappa_1 \nabla T_1 - \nabla \left(\frac{\zeta^2}{2} S_1 \right) - \nabla (\zeta T_1) \right] + \nabla \left\{ \frac{\partial \zeta}{\partial t} (T_1 + \zeta S_1) + (\kappa_1 - \zeta)(\mathbf{u}_1 \cdot \nabla) T_1 + \frac{1}{2} (\kappa_1^2 - \zeta^2)(\mathbf{u}_1 \cdot \nabla) S_1 + \frac{1}{2} [(T_1 + \zeta S_1)^2] \right\} - \mathbf{R}_b + \mathbf{R}_f + \nu_T \left[\nabla S_1 - \nabla^2 \mathbf{u}_1 - \nabla^2 \left(\frac{\kappa_1^2}{2} \nabla S_1 + \kappa_1 \nabla T_1 \right) + \nabla \left(\frac{\zeta^2}{2} \nabla^2 S_1 + \zeta \nabla^2 T_1 \right) \right] = 0 \tag{2}$$

$$\mathbf{u}_2 + \frac{\kappa_2^2 - \eta^2}{2} \nabla S_2 + (\kappa_2 - \eta) \nabla T_2 = \mathbf{u}_1 + \frac{\kappa_1^2 - \eta^2}{2} \nabla S_1 + (\kappa_1 - \eta) \nabla T_1 \tag{3}$$

where

$$S_2 = \nabla \cdot \mathbf{u}_2, \quad T_2 = \nabla \cdot (h\mathbf{u}_2)$$

$$S_1 = \nabla \cdot \mathbf{u}_1, \quad T_1 = \eta(S_2 - S_1) + T_2 \tag{4}$$

$\mathbf{R}_b$=breaking-related dissipation term; $\mathbf{R}_f$ accounts for bottom friction; ν_T=constant eddy viscosity; $\nabla^2 = (\partial^2/\partial x^2 + \partial^2/\partial y^2)$; $\kappa_1 = -0.127h$=evaluation level for the velocity $\mathbf{u}_1$; $\eta = -0.266h$ =layer interface elevation; $\kappa_2 = -0.618h$=evaluation level for the velocity $\mathbf{u}_2$; and ζ=free surface elevation. It is noted that with the choice of $\kappa_1 = -0.531h$ and $\eta = \kappa_2 = -h$, the resulting two equation model becomes equivalent to the highly nonlinear Boussinesq-type model presented by Liu (1994). Also derived by Wei et al. (1995), this highly nonlinear model will be referred to as the one-layer model in this paper. For clarity, the two-layer model is the high-order model, and the one-layer model is the typical-order model.

The two-layer equation model was analyzed in depth in Lynett and Liu (2004a), and will not be repeated here. The resulting linear properties of the two-layer model are shown in Fig. 1, as are the properties of the one-layer model. The numerical scheme used to solve the equation system is a fourth-order, predictor-corrector method for the time integration, with spatial derivatives

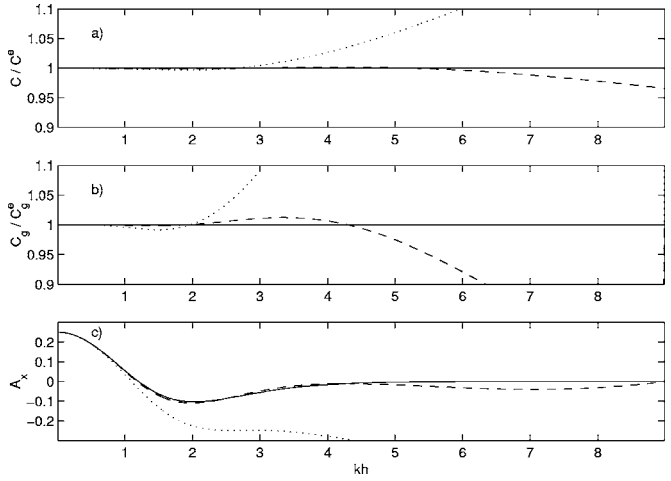

Fig. 1. Linear accuracy of two-layer model. In each plot, solid line is linear theory, dotted line is one-layer model, and dashed line is two-layer model. Subplot (a) shows comparison of phase velocity; (b) group velocity; and (c) shoaling gradient as given by $a_x/a = A_x h_x/h$, where a=wave amplitude and h=water depth.

finite differenced to fourth-order accuracy on a regular grid. Complete details of the numerical model can be found in Lynett and Liu (2004a).

As can be seen in Eq. (2), there are three sources of dissipation: bottom friction, breaking, and constant eddy viscosity dissipation. Bottom friction is calculated with the quadratic friction equation

$$\mathbf{R}_f = \frac{f}{h + \zeta} \mathbf{u}_b |\mathbf{u}_b| \tag{5}$$

where $\mathbf{u}_b$=velocity evaluated at the seafloor; and f=bottom friction coefficient, typically in the range of 10^{-3}–10^{-2}. As noted in Lynett et al. (2002), maximum runup is sensitive to the value of f, particularly for very large, breaking waves: a conservative value of 10^{-3} is used for all simulations here. To simulate the effects of wave breaking, the eddy viscosity model of Kennedy et al. (2000) is used here with some modification. The first modification regards the manner in which a breaking event is initiated. A range of breaking simulations were undertaken including regular wave breaking on a planar slope (Hansen and Svendsen 1979), cnoidal wave breaking on a planar slope (Ting and Kirby 1995), and wave breaking over a submerged breakwater (Dingemans 1994). All of these simulations have experimental data indicating the breaking locations. To determine the best breaking indicator in the numerical model, a number of possible 1HD threshold parameters were investigated, including ζ_t/c, ζ_x, $u_{S_{xx}} H^2/c$, and u_S/c, where u_S=free surface speed (as evaluated from the extended-Boussinesq vertical profile of horizontal velocity); c=local nonlinear long wave speed=$\sqrt{gH}$; H=total water depth=$\zeta + h$; and the subscripts x and t indicate partial derivatives with respect to time and space. Note that simulations using the linear phase speed and the local depth as scaling factors were attempted as well. The results of this analysis are that ζ_x is the least sensitive breaking threshold, with the correct breaking location predicted by $\zeta_x = 0.6 \mp 0.02$ using the two-layer model. The other results showed correct breaking initialization as $\zeta_t/c = 0.55 \mp 0.06$, $u_{S_{xx}} H^2/c = 0.62 \mp 0.05$, and $u_S/c = 0.40 \mp 0.06$. Therefore, wave slope should be used as the breaking model trigger, as has been commonly employed (e.g., Schäffer et al. 1993). It must be noted

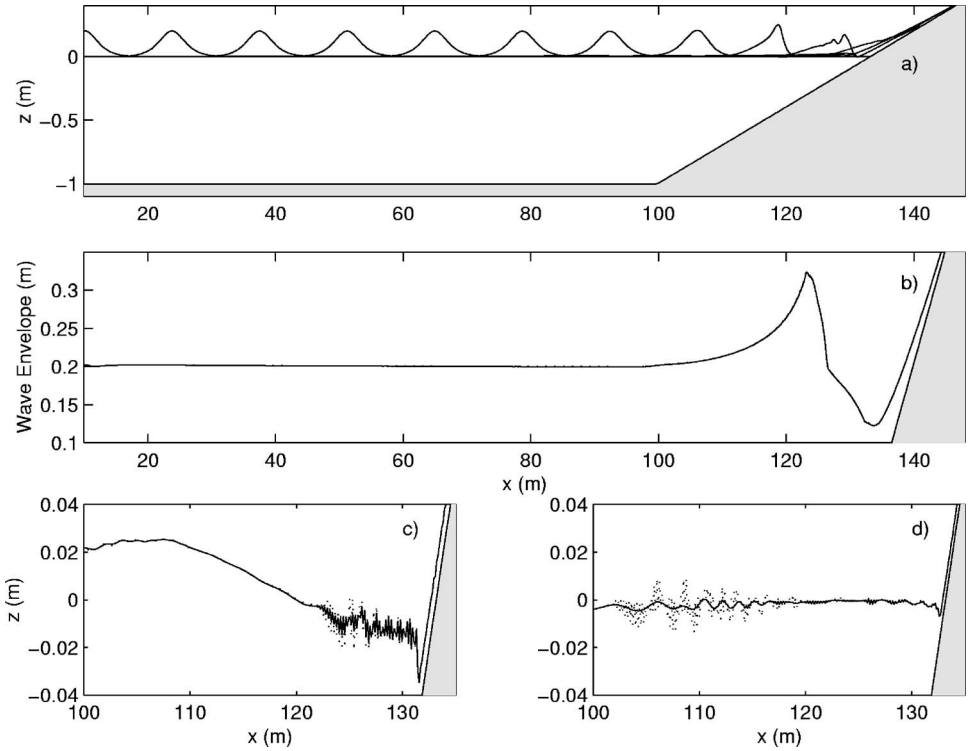

Fig. 2. Solitary wave breaking and runup. Subplot (a) shows waveform at various times; (b) gives wave envelope from simulation with viscosity (solid line) and simulation without viscosity (dotted line); and (c) and (d) are closeups near beach, where two simulations are given as in subplot (b). Subplot (c) is at earlier time than (d), and both are during rundown phase. Positive wave shown in (c) is reflection moving away from beach, and has left frame by (d). Solid seafloor is gray.

here, however, that these coefficients will be specific to the nonlinear-dispersive properties of a given model (here the two-layer model), and care must be taken when employing these thresholds in alternative models.

Through testing with various dissipation models, it was found that, in terms of stability and lack of numerical noise generation, the eddy viscosity model of Kennedy et al. (2000) was preferred for this particular numerical scheme. For the dissipation under a breaking event, modifications to Kennedy et al. are concerned primarily with reformulating the model thresholds in terms of the total water depth, H. In Kennedy et al. thresholds are given in terms of h, making the simulation of breaking uprush, where h is negative, unclear. The structure of the dissipation formulation is identical to Kennedy et al. although the calibrated threshold values are modified. The complete formulation for $\mathbf{R}_b$ is given in Appendix II.

The final dissipation term in Eq. (2), with the leading coefficient ν_T, has not explicitly been included in Boussinesq-type models to date. This term arises when including eddy viscosity in the Navier–Stokes equations, which are the primitive equations used to derive the Boussinesq. A brief Boussinesq model derivation, showing the inclusion of the eddy viscosity, is given in Appendix I. Leading-order dissipation from this term exists for 2HD simulations only and is related to the horizontal gradient of vertical vorticity, which due to the irrotational foundations of the Boussinesq derivation, should be small. However, with the inclusion of bottom friction and wave breaking, this is not necessarily the case. The second-order terms in this expression are related to the fourth-order spatial derivatives of velocity, which should also be small. It is interpreted that this term accounts for the eddy dissipation that is not included in the breaking and bottom friction models. Through simulation testing, an eddy viscosity of $\nu_T=0.001h_0\sqrt{gh_0}$ is used here, where h_0 is a characteristic water depth of the initial condition. This value was found to not have significant impact on the wave field when numerical short waves are not present.

To show the effectiveness of this dissipation term an example simulation is given here. In the numerical model, when a large amplitude solitary wave breaks and runs up a slope, it is common for a small amount of numerical noise to be generated during the rundown phase when bottom friction is not included or small. The reason for this is a very steep, nearly stationary hydraulic jump at the base of the rundown, which propagates out short waves as numerical dispersive errors. For this example simulation, a bottom friction coefficient of $f=0.0001$ is used. Fig. 2 gives four subplots of the solitary wave runup, showing spatial profiles from simulations with $\nu_T=0$ and $\nu_T=0.003$ m^2/s (as calculated from the recommended equation with $h_0=1$ m). Properties of the simulation are nondimensional wave height=0.2, beach slope=1/35, and $\Delta x/h_0=0.1$. The added dissipation has no effect on the wave propagation and runup [Fig. 2(b)], however the rapid damping of the rundown-created short waves is clear as shown in Figs. 2(c and d). Essentially, this new dissipation model represents a somewhat physical means of filtering out unwanted short wave energy.

Experimental Comparisons and Discussion

In this section, a range of 1HD simulations are compared. The focus is on wave characteristics near the breakpoint and through the surf zone. The nearshore impact of using a model with good

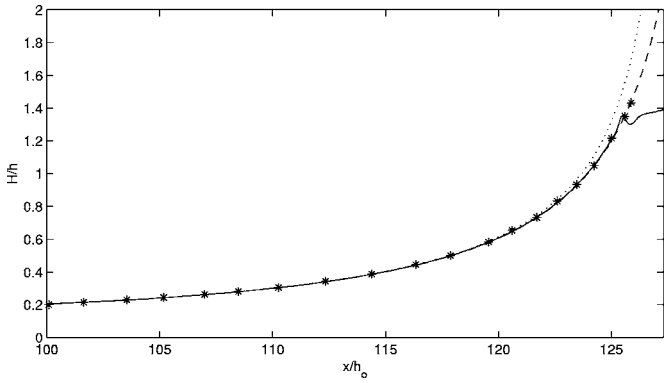

Fig. 3. Shoaled solitary wave height, H, scaled by local water depth, h, versus horizontal location, where h_0=depth at base of slope. Dotted line is one-layer model without breaking; dashed line is two-layer model without breaking; solid line is two-layer model with breaking; and stars are potential flow results as presented in Wei et al. (1995). Last shown star (at x/h_0=125.9) is break point predicted by potential flow model.

short wave properties will be discussed. The numerical grid and time steps for all simulations are given in Appendix III, "Numerical Simulation Parameters."

1HD Wave Breaking on Constant Slope

For an initial comparison, the solitary wave of Fig. 2 is examined more closely. Solitary wave shoaling, up to the break point, was investigated with a potential flow model by Grilli et al. (1994) and then compared with the fully nonlinear Boussinesq model of Wei et al. (1995), a one-layer model. In general, the Boussinesq model predicted shoaling correctly, in agreement with the potential flow model, until very near the break point where the wave overshoals. The two-layer model is compared with the potential flow results, as given in Wei et al. (1995), in Fig. 3. The two-layer model predicts the near-break point shoaling better, however the break point is a bit early. This example provides some confidence that the two-layer model very accurately captures shoaling to near the break point.

Regular wave breaking up a planar slope is examined now. The setup here is taken from Hansen and Svendsen (1979). The depth near the wavemaker from these trials is 0.36 m, leading to a beach slope of 1:34.26. Five cases will be compared, with varying wave period and amplitude. Both wave height and mean water level data is available from the experiments. Fig. 4 gives the results from the one- and two-layer models, as well as the experimental data. A very clear trend appears: the one-layer model overshoals the wave near the breakpoint, while the two-layer model shoals at a rate more consistent with the experimental data. The overshoaling of the one-layer model has been noted previously (e.g. Kennedy et al. 2000), and is an expected property of the one-layer model.

With the two-layer model exhibiting very good accuracy for these cases, we have a mechanism for determining how the one-layer model overshoals the wave. By plotting the behavior of the various harmonics in the wave train, the source of the error becomes apparent. Fig. 5 gives the trends of various harmonics from the one- and two-layer models. In this figure are given three curves for each simulation, showing the combined spectral amplitudes in three harmonic groups: the first harmonic (A_1), the second through fourth harmonics (A_{2-4}), and the fifth and higher

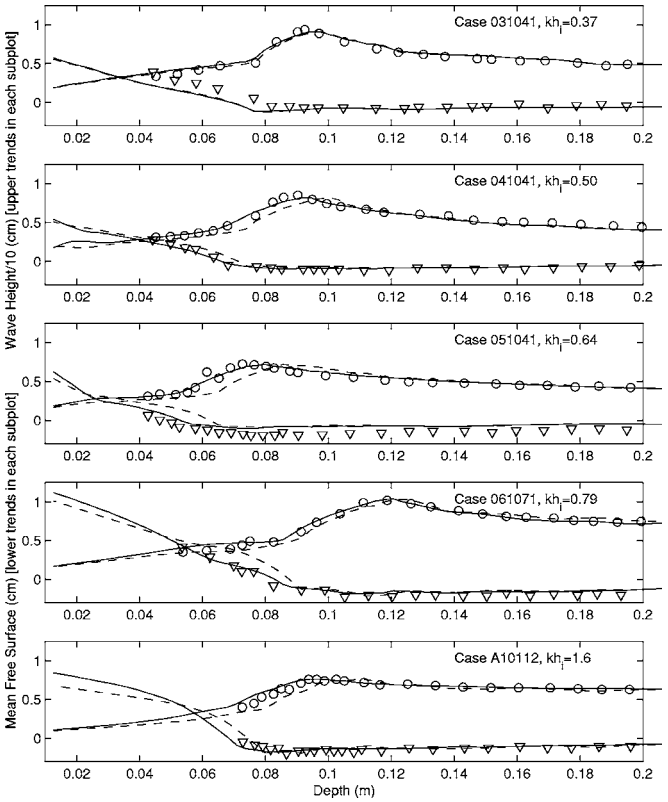

Fig. 4. Wave height and setup comparisons with regular wave breaking experiments of Hansen and Svendsen (1979). Each figure gives kh value of wave at wavemaker, symbols are experimental data, dashed line is one-layer model, and solid line is two-layer model. Top trends in each subplot are wave height and lower trends are mean water level.

harmonics (A_{5+}). These harmonics are grouped as such because the harmonics in each group behaved similarly. Interestingly, both models show significant spectral energy into the tenth harmonic, particularly in the inner surf.

Evident from this comparison is that the overshoaling in the one-layer model is due to over amplification of the fifth and higher harmonics (note that $kh \approx 2$ for the fifth harmonic near the break point). The very high order nonlinear interactions creating these harmonics are, expectedly, not described properly in the one-layer model. Additionally, the break point appears to be controlled by the fifth and higher harmonics, which exhibit an rapid increase in amplitude near the break point, while A_1 shows a nearly linear decrease and A_{2-4} show a linear increase before breaking. To achieve excellent hydrodynamic predictions near the breaking point, a model with correct high-order nonlinear behavior is needed.

Next, cnoidal wave breaking over a constant slope is examined. The data by Ting and Kirby for plunging (1995) and spilling (1996) is used here. This data have been used most frequently to test turbulence generation in numerical models more sophisticated than the one used here (e.g., Lin and Liu 1998; Zhao et al. 2004). However, the wave height data obtained during the experiments are also an excellent benchmark for depth-integrated models in the surf zone (Bredmose et al. 2004). It is noted that, for the cnoidal wave cases, the location of the numerical wavemaker (internal source wave generator), does play a role in the break point location. The reason for this is that, due to the high nonlinearity of the incident wave condition, free waves tended to be generated

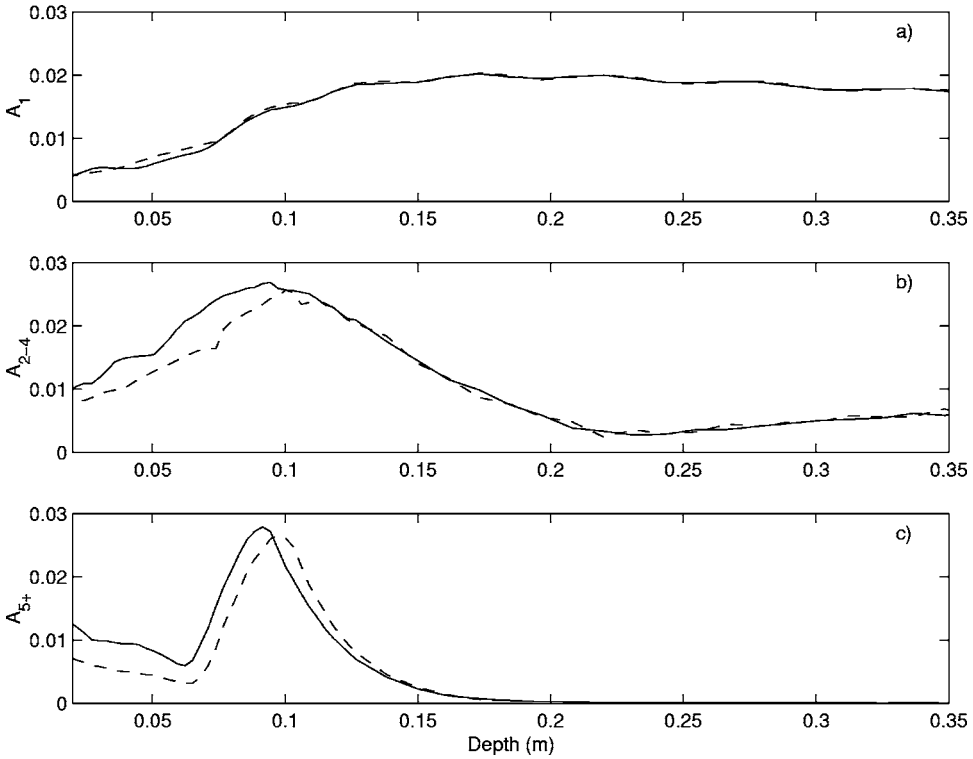

Fig. 5. Amplitudes in harmonic bins as predicted by one-layer (dashed line) and two-layer (solid line) model for case 041041 shown in Fig. 4. In (a) is first harmonic amplitude, A_1, in (b) is sum of second through fourth, $A_{2-4}=\Sigma_{n=2}^{4}A_n$, and in (c) sum of fifth and higher harmonics, $A_{5+}=\Sigma_{n=5}^{\infty}A_n$.

with the cnoidal wave train, which would then interact in a nonlinear manner. Depending on the interaction time possible for the wave components, which is controlled by the wavemaker location, the breakpoint could be shifted. Care was taken to ensure that the numerical wavemaker was at the same location as the experimental. The numerical–experimental comparisons for the spilling and plunging breakers are given in Figs. 6 and 7, respectively. Shown in these comparisons is a trend similar to that already mentioned: the one-layer model shoals much more rapidly near the break point, and apparently much less realistically. This is the case in particular for the plunging breaker, where the one-layer model predicts substantially different crest levels near the break point and the outer surf zone. Interestingly, the mean water level and the trough level as predicted by the one-layer model is quite good, in agreement with both the two-layer model and the experiment. This is an indication that, at least for these cnoidal wave cases, the mean water level and the trough level are not sensitive to high-order nonlinear and dispersion accuracy, while the crest level is. Also worthy of note is that in the inner surf zone, the numerical predictions converge, which is a likely sign that breaking is becoming a depth-limited process in this region.

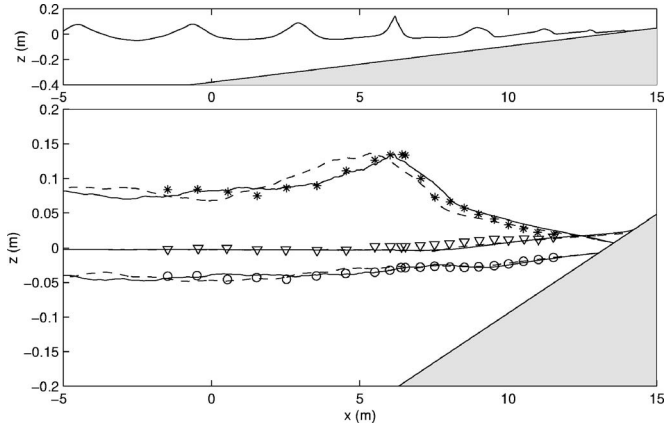

Fig. 6. Comparisons with experimental data from Ting and Kirby spilling breaker. In top subplot, snapshot of numerical simulation is given. Below experimental crest level (stars), trough level (circles), and mean water level (triangles) are shown, as well as corresponding values from one-layer model (dashed line) and two-layer model (solid line).

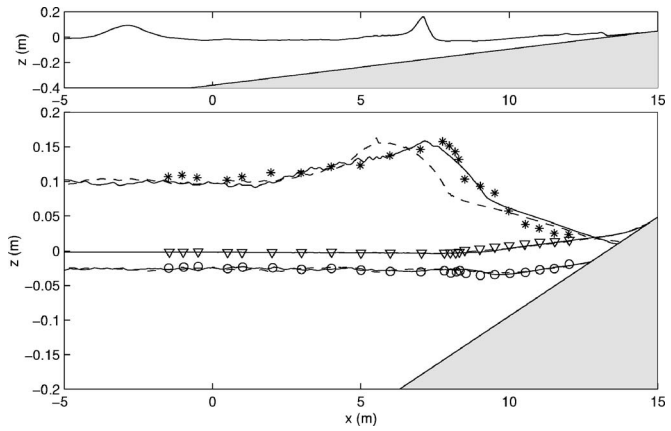

Fig. 7. Comparisons with experimental data from Ting and Kirby plunging breaker. Figure setup same as in Fig. 6.

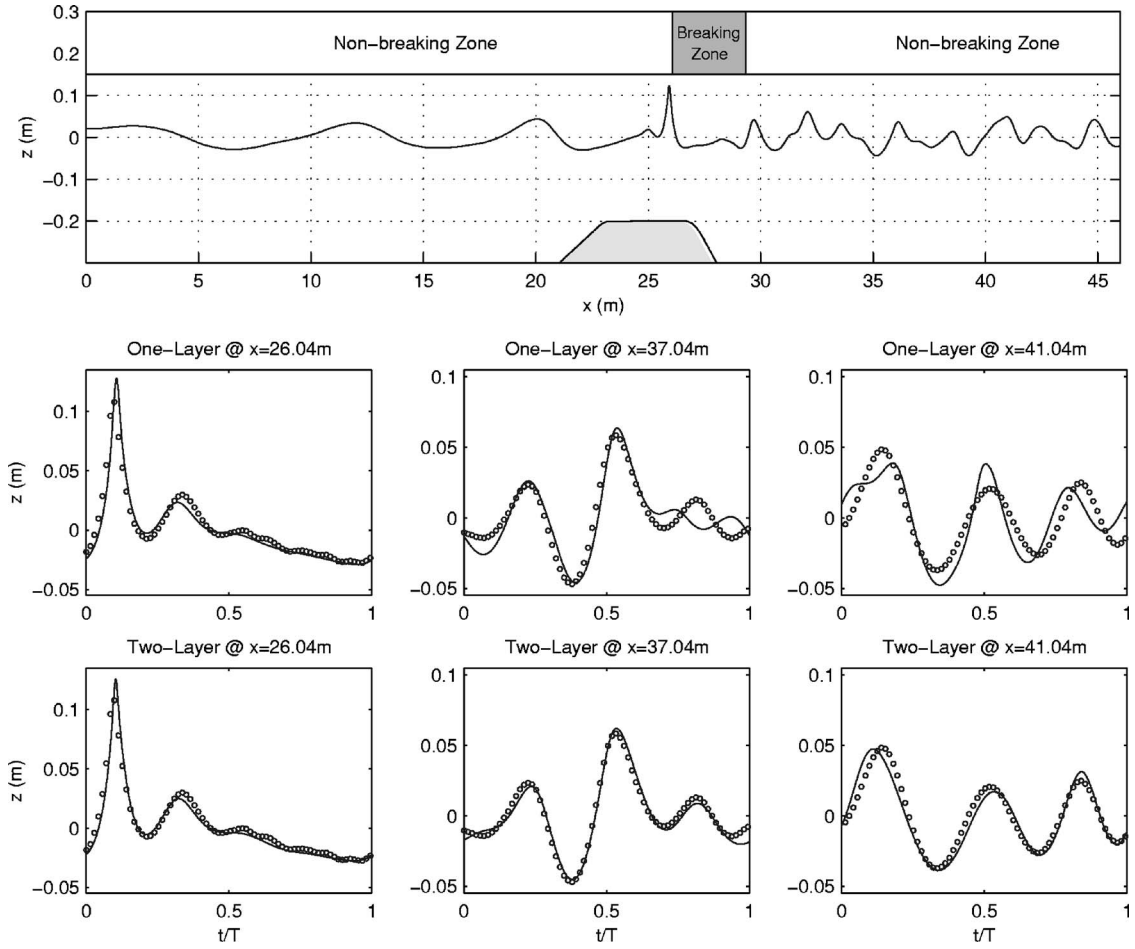

Fig. 8. Comparison with experimental data from Dingemans submerged step. Top subplot gives snapshot of numerical free surface, as well as breaking region. Middle row gives one-layer comparisons and last row gives two-layer comparisons. One- and two-layer results are given with solid lines and experimental data with circles.

1HD Wave Breaking over Bar

As described in Kennedy et al. (2000), the breaking initiation criteria for the eddy viscosity breaking model, stated in terms of η_t, depends on whether the wave is breaking on a constant slope (as discussed above) or breaking over a bar-type feature. With the modifications given in this paper, including the breaking initiation given in terms of local free surface slope, this does not appear to be the case. The single recommended value works for both slope and bar tests. Here, the numerical models are compared with the submerged step experiments presented by Dingemans (1994). Note that this is the same setup as reported in Luth et al. (1994). The bathymetry is composed of a wavemaker depth of 0.86 m leading to a step with a front side slope of 1/20, a back slope of 1/10, and a minimum depth above the step of 0.2 m. The incident wave condition is $kh=0.55$ with an nondimensional amplitude of $a/h=0.072$.

For this case, both the one- and two-layer models are run. Fig. 8 summarizes the results and gives the experimental comparisons. The top subplot shows a snapshot of the free surface, and also gives the breaking region. The experimentally observed breaking region between $x=26$ and 29 m matches the numerically predicted region very well. Note that for the numerical models to reach convergence, an extremely fine grid was required: 400 points per wave at the wavemaker, or $dx=0.024$ m. The reason for this required very fine grid is that, for this case, the breaking threshold is just barely met, requiring a very precise evaluation of the wave slope. Using a more practical resolution, 100 points per incident wave (which gives roughly 10 points in the crest immediately before breaking), similar accuracy is achieved with the breaking initiation reduced to $\zeta_x=0.5$.

Looking to the free surface comparisons in Fig. 8, the two-layer model shows higher agreement with experiment behind the bar. This increase in agreement is related to the release of locked higher harmonics after the wave breaks and passes into the deep water behind the bar. Once free, these higher harmonics travel according to the linear dispersion relation, which the one-layer model predicts inaccurately for the third and higher harmonics (third harmonic has $kh=2.5$ behind the bar).

Random Wave Breaking

In this section, the numerical model is compared with field data obtained during the SwashX experiments (Raubenhiemer 2002). The beach profile is shown in the top plot of Fig. 9. Here, the spectral transformation as well as the wave height through the surf zone are examined. A 15 min segment of the recorded field data is recreated numerically. The numerical recreation uses as input the spectral decomposition of the field data, which is a linear superposition of many frequencies with varying amplitude.

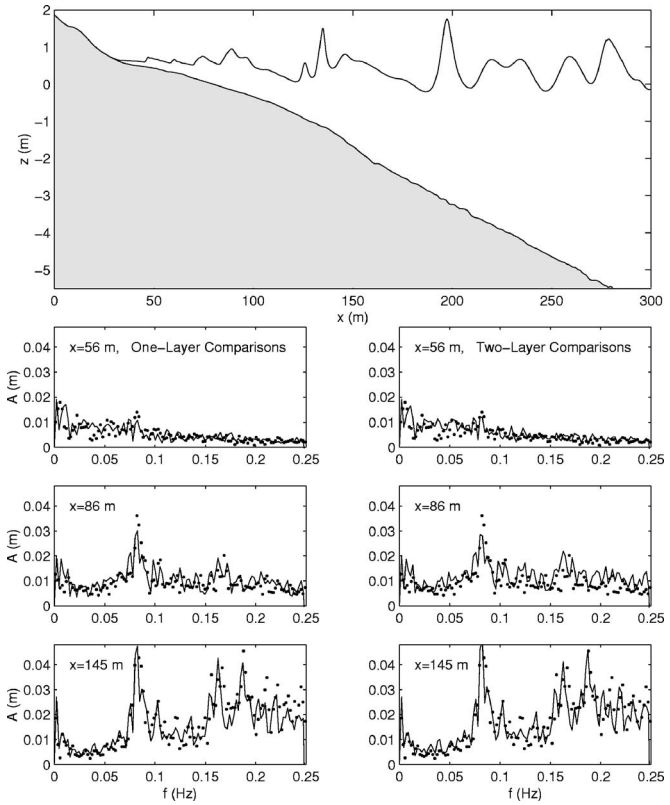

Fig. 9. Comparison with SwashX field data. Top plot shows spatial snapshot from two-layer model, where measured beach profile is given in grey. Lower subplots compare discrete amplitude spectrums at different locations from numerics (solid line) and measured data (dots), where one-layer comparisons are on left and two-layer are on right. All spectrums use identical frequency spacings and are filtered.

Thus, the numerical recreation suffers with this linear superposition, as most certainly some of the field energy is locked.

In the lower subplots of Fig. 9, spectral comparisons with the numerical and field data are made, for both the one- and two-layer models. Two items become evident: (1) the Boussinesq-type model with the employed breaking scheme does a very good job at capturing the spectral transformation through the surf zone including infragravity wave energy, and (2) the one- and two-layer models show equivalent agreement in light of the accuracy of the field data and the uncertainty in the numerical wave input condition.

While the above discussion looks at the detail of the wave field, it is also useful to examine the mean quantities. Fig. 10 compares mean surface and significant wave height. Again both models do a reasonable job at recreating the field site. The trends in wave height mimic previously analyzed data, with the two-layer model predicting larger values in the outer surf, due to better shoaling representation and a break point in shallower water. While the differences between the model results are clear and arguably significant, this comparison indicates that the errors in the one-layer model are likely on the order of those associated with the ability to recreate field conditions and in the measured field data itself. However, the two-layer model has a demonstrated higher accuracy, and preference should be given to its use when practical.

Conclusions

A slightly modified version of the eddy viscosity breaking model (Kennedy et al. 2000) is employed here in a high-order Boussinesq-type model: the two-layer model of Lynett and Liu (2004a). Numerous simulations are run and compared with the highly nonlinear Boussinesq-type model, or the one-layer model.

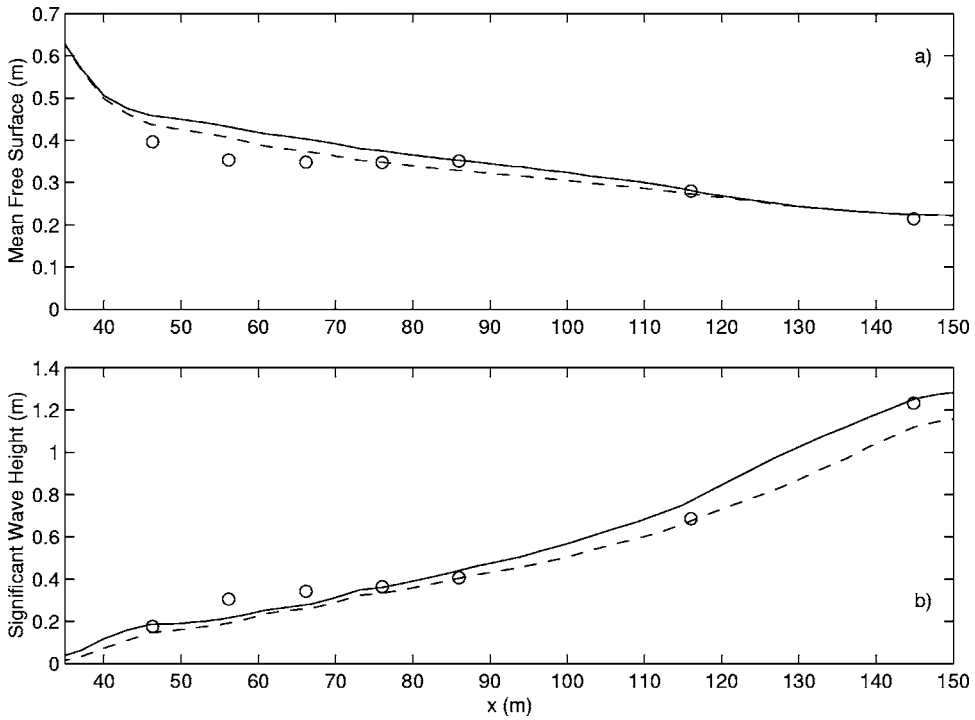

Fig. 10. Numerical-field comparisons between mean free surface (a) and wave height (b). Measured data are given by circles; one-layer model by dashed line; and two-layer model by solid line. x coordinate is same as shown in Fig. 9.

The documented over-shoaling of the one-layer model for regular waves is shown to be due to an overamplification of the fifth and higher harmonics in a region immediately seaward of breaking. These high-order nonlinear components are better captured in the two-layer model, which exhibits closer agreement with experimental data for both monochromatic and cnoidal waves. With wave breaking over a step, breaking does start using a single initiation threshold parameter for both step and slope breaking. Better accuracy is seen in the two-layer model behind the step, where high kh waves propagate as free waves. Finally, the SwashX field conditions are recreated approximately, and the Boussinesq-type model shows its ability to capture the spectral transformation of a wave field through the surf zone, without favoring the higher-order model.

Acknowledgments

The writer would like to thank Dr. Britt Raubenhiemer for providing the raw data from the SwashX experiments, which were funded by the Office of Naval Research. The research presented here was partially supported by a grant from the National Science Foundation (Grant No. CTS-0427115).

Appendix I. Inclusion of Viscosity Terms in Boussinesq Derivation

The goal of this section is to derive a set of equations by integrating the primitive equations of motion in the vertical direction. The sole difference between this derivation, and that given in Lynett and Liu (2004a), is that the viscosity term is not truncated in the momentum equations. It is noted that although the derivation presented here employs just two layers, the procedure is directly extendable to any arbitrary number of layers (Lynett and Liu 2004b). The flow region is divided by an interface, $z'=\eta'$. The resulting upper layer has a characteristic thickness d_1 (all variables contained entirely in this layer will be denoted with the subscript "1"), while the lower layer has a thickness d_2 (variables in this layer denoted by the subscript "2"). The determination of the location of the interface constitutes a part of the formulation of the model equations. Utilizing the layer thicknesses d_1 and d_2 as the vertical length scales in the upper and lower layer, respectively, the characteristic length of the wave l_0 as the horizontal length scale, h_0 as the characteristic water depth, $l_0/\sqrt{gh_0}$ as the time scale, and the characteristic wave amplitude a_0 as the scale of wave motion, we can define the following dimensionless variables:

$$(x,y)=(x',y')/l_o,\quad z_n=z'/d_n,\quad t=\sqrt{gh_0}t'/l_o$$

$$h=h'/h_0,\quad \zeta=\zeta'/a_o,\quad \eta=\eta'/d_1$$

$$(U_n,V_n)=(U_n',V_n')/(\varepsilon_o\sqrt{gh_0}),\quad W_n=W_n'/(\varepsilon_o\mu_o\sqrt{gh_0})$$

$$p_n=p'/\rho g a_o \tag{6}$$

in which the subscript $n=1,2$ indicates the layer index; (U_n,V_n) represent the horizontal velocity components in the different layers; W_n=vertical velocity component; and p_n=pressure. Note that the vertical coordinate, z_n, is scaled differently in each layer. Two dimensionless parameters have been introduced in Eq. (6), i.e.

$$\varepsilon_o=a_o/h_0,\quad \mu_o=h_0/l_o \tag{7}$$

Assuming that the viscous effects are not insignificant, the wave motion can be described by the continuity equation and the Navier–Stokes equation, i.e.

$$\frac{d_n}{h_0}\nabla\cdot\mathbf{U}_n+\frac{\partial W_n}{\partial z_n}=0 \tag{8}$$

$$\frac{\partial\mathbf{U}_n}{\partial t}+\varepsilon_o\mathbf{U}_n\cdot\nabla\mathbf{U}_n+\varepsilon_n W_n\frac{\partial\mathbf{U}_n}{\partial z_n}=-\nabla p_n+\nu_n\nabla_n^2\mathbf{U}_n \tag{9}$$

$$\mu_n^2\left(\frac{\partial W_n}{\partial t}+\varepsilon_o\mathbf{U}_n\cdot\nabla W_n\right)+\varepsilon_o\mu_o^2W_n\frac{\partial W_n}{\partial z_n}=-\left(\frac{\partial p_n}{\partial z_n}+\frac{1}{\varepsilon_n}\right)+\mu_n^2\nu_n\nabla_n^2W_n \tag{10}$$

where $\mu_n^2=d_nh_0/l_o^2$; $\varepsilon_n=a_o/d_n$; $\mathbf{U}_n=(U_n,V_n)$ denotes horizontal velocity vector; $\nabla=(\partial/\partial x,\partial/\partial y)$=horizontal gradient vector; $\nabla_n^2=(\partial^2/\partial x^2+\partial^2/\partial y^2+l_o^2/d_n^2\partial^2/\partial z_n^2)$; and ν_n=dimensionless, layer dependent viscosity equal to $\nu_n'/(l_o\sqrt{gh_0})$; where ν_n'=dimensional viscosity. It is remarked here that ν_n' will eventually be specified through a eddy viscosity type formulation.

Derivation of the vertical profiles of velocity and the approximate continuity equation are based only on Eq. (8) and boundary conditions, and are thus unchanged from that given in Lynett and Liu (2004a). The eddy viscosity included in the primitive equations above is interpreted as acting in the body of the fluid, away from the boundaries. The bottom friction model given in Eq. (5) is expected to approximately include bottom boundary layer dissipation. It is not sought here to modify the bottom boundary condition such that the velocity profile in this region is better modeled, as done in Liu and Orfila (2004).

Working through the perturbation Boussinesq derivation, with the assumption of a constant eddy viscosity in space, the pressure profile in the upper layer is modified to

$$p_1=\zeta-\frac{z_1}{\varepsilon_1}+\mu_1^2\{\dots\}+\mu_n^2\nu_n\left\{\frac{1}{2}(\varepsilon_1^2\zeta^2-z_1^2)\nabla^2S_1+(\varepsilon_1\zeta-z_1)\nabla^2T_1\right\}+O(\mu_o^2\mu_n^2,\mu_n^4),\quad \eta<z_1<\varepsilon_1\zeta \tag{11}$$

where $\nabla^2=(\partial^2/\partial x^2+\partial^2/\partial y^2)$. This pressure profile leads to the new momentum equation

$$\frac{\partial\mathbf{u}_1}{\partial t}+\frac{\varepsilon_o}{2}\nabla(\mathbf{u}_1\cdot\mathbf{u}_1)+\nabla\zeta+\mu_1^2\{\dots\}+\nu_n\left[\frac{h_0}{d_1}\nabla S_1-\nabla^2\mathbf{u}_1-\mu_n^2\nabla^2\left(\frac{\kappa_1^2}{2}\nabla S_1+\kappa_1\nabla T_1\right)+\mu_n^2\nabla\left(\frac{1}{2}\varepsilon_1^2\zeta^2\nabla^2S_1+\varepsilon_1\zeta\nabla^2T_1\right)\right]=O(\mu_o^2\mu_1^2) \tag{12}$$

In the above equations the neglected terms in the {…} can be found in Lynett and Liu (2004a), or any highly nonlinear extended Boussinesq derivation.

Appendix II. Wave Breaking Formulation

The breaking term in the momentum equation is given by $\mathbf{R}_b=[R_{bx},R_{by}]$, where

$$R_{bx}=\frac{1}{H}\{[\nu(Hu_1)_x]_x+0.5[\nu(Hu_1)_y+\nu(Hv_1)_x]_y\} \tag{13}$$

$$R_{by}=\frac{1}{H}\{[\nu(Hv_1)_y]_x+0.5[\nu(Hu_1)_y+\nu(Hv_1)_x]_x\} \tag{14}$$

The viscosity, ν, is

$$\nu=B\delta^2H\zeta_t \tag{15}$$

where

$$B=\begin{cases}1, & \zeta_t\geqslant 2\zeta_t^*\\ \zeta_t/\zeta_t^*-1, & \zeta_t^*<\zeta_t\leqslant 2\zeta_t^*\\ 0, & \zeta_t\leqslant\zeta_t^*\end{cases}$$

and

$$\zeta_t^*=\begin{cases}\zeta_t^F, & t-t_0\geqslant T^*\\ \zeta_t^I+\dfrac{t-t_0}{T^*}(\zeta_t^F-\zeta_t^I), & 0\leqslant t-t_0<T^*\end{cases}$$

To this point, the formulation, as given by the above equations, is identical to that presented by Kennedy et al. (2000). For the two-layer model, the following parameter values are found to yield the best agreement with experiment:

$$\delta=10,\quad T^*=10\sqrt{H/g},$$

$$\zeta_t^I=0.5\sqrt{gH},\quad \zeta_t^F=0.05\sqrt{gH} \tag{16}$$

Furthermore, breaking cannot initiate unless

$$\sqrt{\zeta_x^2+\zeta_y^2}\geqslant 0.60 \tag{17}$$

This criteria is enforced by first checking if the wave in question is already breaking; if it is not, the slope threshold must be met for any further breaking model calculations to be performed. The breaking model is utilized in a semiexplicit manner, meaning that the viscosity at time level $n+1$ is calculated with ζ values from time level n. The remaining terms in $\mathbf{R}_b$ are calculated in an implicit manner. It is reiterated here that the above parameter set is tuned for the two-layer model, and transfusion of these parameters into a different model with different nonlinear properties will likely yield different results.

Appendix III. Numerical Simulation Parameters

Table 1 provides the incident water depth (h_0), wavelength (L_o), constant grid length (Δx), and time step (Δt) for all results presented in this paper.

Table 1. Numerical Simulation Parameters.

	h_0 (m)	L_o (m)	Δx (m)	Δt (s)
Solitary wave (Fig. 2)	1.0	≈7	0.10	0.020
H-S 031041 (Fig. 4)	0.36	6.1	0.012	0.0035
H-S 041041 (Fig. 4)	0.36	4.5	0.012	0.0035
H-S 051041 (Fig. 4)	0.36	3.5	0.012	0.0035
H-S 061071 (Fig. 4)	0.36	2.9	0.012	0.0035
H-S A10112 (Fig. 4)	0.36	1.4	0.012	0.0035
T-K spiller (Fig. 6)	0.40	5.3	0.026	0.0067
T-K plunger (Fig. 7)	0.40	15	0.030	0.0077
Submerged step (Fig. 8)	0.86	9.9	0.024	0.0043
SwashX (Fig. 9)	6.7	≈70	0.34	0.021

References

Agnon, Y., Madsen, P. A., and Schäffer, H. (1999). "A new approach to high order Boussinesq models." *J. Fluid Mech.*, 399, 319–333.

Basterretxea, G., Orfila, A., Jordi, A., Casas, B., Lynett, P., Liu, P. L.-F., Duarte, C. M., and Tintor, J. (2004). "Seasonal dynamics of a microtidal pocket beach with posidonia oceanica seabeds (Mallorca, Spain)." *J. Coastal Res.*, 20(4), 1155–1164.

Beji, S., and Battjes, J. A. (1994). "Numerical simulation of nonlinear waves propagation over a bar." *Coastal Eng.*, 23, 116.

Bredmose, H., Schäffer, H. A., and Madsen, P. A. (2004). "Boussinesq evolution equations: numerical efficiency, breaking and amplitude dispersion." *Coastal Eng.*, 51(11–12), 1117–1142.

Chen, Q., Kirby, J. T., Dalrymple, R. A., Shi, F., and Thornton, E. B. (2003). "Boussinesq modeling of longshore currents." *J. Geophys. Res.*, 108(C11), 3362.

Dingemans, M. (1994). "Comparison of computations with Boussinesq-like models and laboratory measurements." *Mast-G8M Note No H1684*, Delft Hydraulics, Delft, The Netherlands.

Gobbi, M. F., Kirby, J. T., and Wei, G. (2000). "A fully nonlinear Boussinesq model for surface waves. Part II: Extension to $O(kh)^4$)." *J. Fluid Mech.*, 405, 182–210.

Grilli, S. T., Subramanya, R., Svendsen, I. A., and Veeramony, J. (1994). "Shoaling of solitary waves on plane beaches." *J. Waterw., Port, Coastal, Ocean Eng.*, 120(6), 609–628.

Hansen, J. B., and Svendsen, I. A. (1979). "Regular waves in shoaling water: Experimental data." *Tech. Rep. ISVA Ser.*, *21*, Technical Univ. of Denmark, Denmark.

Kennedy, A. B., Chen, Q., Kirby, J. T., and Dalrymple, R. A. (2000). "Boussinesq modeling of wave transformation, breaking and runup. I: 1D." *J. Waterw., Port, Coastal, Ocean Eng.*, 126(1), 39–47.

Kennedy, A. B., Kirby, J. T., Chen, Q., and Dalrymple, R. A. (2001). "Boussinesq-type equations with improved nonlinear behaviour." *Wave Motion*, 33, 225–243.

Lin, P., and Liu, P. L.-F. (1998). "A numerical study of breaking waves in the surf zone." *J. Fluid Mech.*, 359, 239–264.

Liu, P. L.-F. (1994). "Model equations for wave propagation from deep to shallow water." *Advances in coastal engineering* P. L.-F. Liu, ed., Vol. 1, World Scientific, Singapore, 125–157.

Liu, P. L.-F., and Orfila, A. (2004). "Viscous effects on transient long wave propagation." *J. Fluid Mech.*, 520, 83–92.

Luth, H. R., Klopman, G., and Kitou, N. (1994). "Project 13G: Kinematics of waves breaking partially on a offshore bar; LDV measurements for wave with and without net onshore current." *Delft Hydraulics Rep. H1573*, Delft, The Netherlands.

Lynett, P., and Liu, P. L.-F. (2004a). "A two-layer approach to water wave modeling." *Proc. R. Soc. London, Ser. A*, 460, 2637–2669.

Lynett, P., and Liu, PL.-F. (2004b). "Linear analysis of the multi-layer model." *Coastal Eng.*, 51(6), 439–454.

Lynett, P., Liu, P.L.-F., Losada, I., and Vidal, C. (2000). "Solitary wave interaction with porous breakwaters." *J. Waterw., Port, Coastal,*

Ocean Eng., 126(6), 314–322.
Lynett, P., Wu, T.-R., and Liu, P. L.-F. (2002). "Modeling wave runup with depth-integrated equations." *Coastal Eng.*, 46(2), 89–107.
Madsen, P. A., Bingham, H. B., and Liu, H. (2002). "A new Boussinesq method for fully nonlinear waves from shallow to deep water." *J. Fluid Mech.*, 462, 1–30.
Madsen, P. A., and Sorensen, O. R. (1992). "A new form of the Boussinesq equations with improved linear dispersion characteristics. Part II: A slowly varying bathymetry." *Coastal Eng.*, 18, 183–204.
Nwogu, O. (1993). "Alternative form of Boussinesq equations for nearshore wave propagation." *J. Waterw., Port, Coastal, Ocean Eng.*, 119(6), 618–638.
Raubenheimer, B. (2002). "Observations and predictions of fluid velocities in the surf and swash zones." *J. Geophys. Res.*, 107, 3190.
Schäffer, H. A., Madsen, P. A., and Deigaard, R. (1993). "A Boussinesq model for waves breaking in shallow water." *Coastal Eng.*, 20, 185–202.
Sorensen, O. R., Madsen, P. A., and Schäffer, H. A. (1999). "Nearshore wave dynamics simulated by Boussinesq-type models." *Proc., ICCE'98*, ASCE, Reston, Va., 272–285.
Ting, F. C.-K., and Kirby, J. T. (1995). "Dynamics of surf-zone turbulence in a strong plunging breaker." *Coastal Eng.*, 24, 177–204.
Ting, F. C. K., and Kirby, J. T. (1996). "Dynamics of surf-zone turbulence in a spilling breaker." *Coastal Eng.*, 27, 131–160.
Wei, G., Kirby, J. T., Grilli, S. T., and Subramanya, R. (1995). "A fully nonlinear Boussinesq model for surface waves. Part 1. Highly nonlinear unsteady waves." *J. Fluid Mech.*, 294, 71–92.
Zhao, Q., Armfield, S., and Tanimoto, K. (2004). "Numerical simulation of breaking waves by a multi-scale turbulence model." *Coastal Eng.*, 51, 53–80.